Autonomous and wireless accelerometers for monitoring bridge stay cables

P. Laurent, P. Bellier, F. Dupont and J.-M. Redouté

***Abstract*—In cable-stayed bridges, the cables are tensioned to support the weight of the deck and the loading. In practice, it is essential to monitor the long-term stability of cable tensions to ensure the structural integrity and safety of the bridge. In this study, we focus on vibration-based analysis, a non-intrusive and easy-to-implement method. Ultimately, the key information lies in extracting the frequency content – at least the fundamental frequency – of the cable vibration from which the cable tension can be derived, much like a guitar tuner. To do so, we have designed an autonomous wireless sensor node (106 × 75 × 41 mm³) that does not require maintenance after placement. The instrumentation part is based on a high-precision 3-axis accelerometer and a temperature sensor. The acceleration is sampled at 250 Hz and processed locally using a Fast Fourier Transform (FFT) implemented on the microcontroller. Even though the sensor node transmits the processed data wirelessly, the raw data is logged in a micro-SD card for redundancy and potential post-analysis. The fundamental frequency and dominant harmonics are transmitted hourly through a LoRa communication with a range exceeding 7 km. The instrumentation and processing have been validated through experimental tests performed on a shaker. The sensor node is powered by a small photovoltaic panel of 28 cm² providing a complete 24/7 autonomy despite an unfavorable orientation (near-vertical, facing north-northeast). The results, benchmarked with a reference instrumentation system, validate this plug-and-play instrumentation.**

***Index Terms*— Accelerometer, Energy Harvesting, Internet of Things, Low-Power Wide Area Networks, Structural Health Monitoring.**

I. Introduction

STRUCTURAL Health Monitoring (SHM) applied to civil engineering structures refers to the assessment of the condition of civil engineering structures (e.g., bridges, dams, wind turbines...) in order to ensure both safety and structural integrity [1][2][3]. Through continuous monitoring, data can be collected and analyzed to develop predictive maintenance tools. Predictive maintenance not only reduces operational costs but also extends the service life and performance of infrastructures [4]. The collapse of the Morandi bridge (Genoa, Italy) in 2018 highlighted the consequences of inadequate structural maintenance [5].

Globally, most critical infrastructures, such as motorway bridges, were built in the 1960s and are now reaching a critical age [6]. It has therefore become essential to monitor their condition closely in order to enable timely and well-planned repairs, or schedule the decommissioning and reconstruction of certain structures based on optimal phasing strategies [7][8]. To this end, sensor nodes are generally installed at specific locations on the structure, enabling data acquisition for subsequent analysis using modeling and/or artificial intelligence techniques. [9][10][11]. In this work, we focus on the monitoring of stay cables in cable-stayed bridges. In 2018, the deck of a cable-stayed bridge located in Belgium suddenly lifted by 65 cm during a night with particularly low temperatures [12]. Road traffic on this key cross-border national road (Belgium–Netherlands) was suspended for several months, causing major disruption for logistics and commuters. The incident could potentially have been avoided if early warning signs or predictive monitoring tools had been in place. The problem is that instrumenting such a structure is complex and costly.

In this study, we will focus on the indirect method of measuring the tension in stay cables based on cable vibration using accelerometers [3][9][11][13][14] which is minimally invasive. An alternative approach consists in using non-contact techniques such as laser vibrometers, microwave radar, or vision-based sensing [15]. In practice, the stay cables are naturally excited by the traffic and/or by environmental factors such as wind and rain [16][17][18][19].

The conventional approach relies on the use of wired sensors [11][19]. This results in a complex and costly installation, difficult maintenance (corrosion or cable breakage), limited flexibility, and a negative impact on the clean aesthetic design of cable-stayed bridges [20][21].

Manuscript received xxx.
xxx.
This work was supported by the Walloon Region of Belgium within the frame of the SCARLETT Project (POC n°23-11 Research Program, convention DIFST 2380066). xxx.
(Corresponding author: Philippe LAURENT.)
The authors are with the Microsys Laboratory, Department of Electrical Engineering and Computer Science, University of Liège, 4000 Liège, Belgium (e-mail: p.laurent@uliege.be).
Digital Object Identifier xxx

An alternative solution consists in deploying wireless sensors. However, accelerometers generate large volumes of data, requiring the use of appropriate communication protocols (e.g., Zigbee, Wi-Fi) [8][22][23][24][25], which are energy-intensive and limited in range. As a result, these wireless sensors are generally powered by bulky batteries that must be replaced periodically. The resulting bulky sensor nodes may alter the vibrational response of the stay cable and undermine visual aesthetics of the structure. Furthermore, the reliability of this method is compromised by the need to transmit a large data stream without losses [22] to one or more gateways nearby (< 100 m) [24][26]. Then, the data still needs to be transferred from the gateway to the cloud using an appropriate protocol [27][28].

The power constraint due to limited battery lifetime is generally addressed by applying energy harvesting (EH) technologies [24][29]. In a recent systematic literature review [29], about half of the presented EH techniques, especially applied to SHM, use vibrations (electromagnetic or piezoelectric conversion) while around a quarter uses a solar cell. Several studies [30][31][32] have demonstrated the potential for exploiting low-level vibrations. However, the expected acceleration levels in our study case (typ. 1 mg) are below one order of magnitude compared to previously listed works, which means that the harvested energy will be largely insufficient to power the sensor node. For this reason, we opted for photovoltaic energy harvesting.

In this work, we have developed autonomous and wireless sensor nodes dedicated for SHM which have been tested successfully in a laboratory as well as in the field. The sensor node comprises a precision accelerometer, a temperature sensor, a LoRa communication module, a microcontroller performing the data processing, a solar cell and a dedicated power management unit. The entire system is housed in a rugged enclosure ($106 \times 75 \times 41$ mm³) for outdoor use. Section II presents the design of the sensor node focusing on the main design parts: instrumentation, communication, power, and packaging. Section III describes the results of tests conducted first in the laboratory, then in the field with the assessment of the main characteristics of the hardware fixed on stay cables. The results are discussed in Section IV and benchmarked with the outputs generated by a conventional method. Finally, the concluding section summarizes the key findings and provides insights into future developments.

II. Sensor Node Design

A. Instrumentation

We aim to monitor the tension T in the stay cables. Following an indirect method, the cable tension can be easily obtained using an accelerometer since there exists a relationship (1) between the n^{th} natural frequency f_n [Hz] and the tension T [N], provided that the linear mass density μ [kg/m] and the cable length L [m] are known [14].

$$T = 4 \cdot \mu \cdot L^2 \cdot \left(\frac{f_n}{n}\right)^2 \quad (1)$$

Eq. (1) is based on the ideal vibrating-string model, which is valid when the lateral displacements are small compared to the length L and the medium is non-damped. These assumptions are reasonably satisfied in our case since the displacements are negligible relative to the cable length (several tens of meters) and the end anchorages do not include any dissipative elements. For more complex use cases, particularly short cables with unknown boundary conditions, advanced methods have been proposed based on the concept of the effective vibration length (EVL) [33]. In a continuous monitoring perspective, we take advantage of the fact that the stay cable will undergo natural vibration when excited by external sources such as traffic, wind, or rain–wind interaction. The weakness of the indirect method – as opposed to the use of a load cell, for instance – is that, in the absence of any external excitation, there is no vibrational signal available to estimate the load. To enable accurate frequency measurement, including at very low vibration amplitudes, the selection of a high-sensitivity accelerometer is therefore critical. Accordingly, a 20-bit MEMS accelerometer is employed for the acceleration measurement.

The expected natural frequency of the cable to be monitored is around a few Hertz. Considering the Shannon theorem (aliasing), and in order to obtain a sufficiently rich harmonic content, we set the sampling rate at 250 Hz (low-pass frequency of 62.5 Hz). The device is configured to wake every hour to acquire a buffer of 8192 points per axis, corresponding to 32.8 seconds at this sampling rate. This allows for a frequency resolution of approximately 0.03 Hz.

Acceleration is acquired along all three axes even though the information along the longitudinal axis is, a priori, less relevant. We define the sensitivity rate (SR) as the percentage of signal sample that yield an exploitable frequency content i.e. a non-zero spectral response. In practice, this rate should be high enough to ensure, in conjunction with the sampling rate, a regular update of tension information, at least 4 times per day. The raw data collected are first stored on a microSD card and then processed by the microcontroller to extract relevant information, specifically the five dominant frequencies. We selected a microSD card as memory to ease raw data extraction for debugging, testing and optimization purposes.

The firmware has been optimized to achieve maximum energy efficiency and to accommodate the CMSIS-DSP Q31 fixed-point 8192-point real Fast Fourier Transform (FFT) within the microcontroller's limited 64 Kbytes RAM. The original implementation was modified to compute directly the squared magnitude of the frequency domain, eliminating the need to store real and imaginary components as well as the complex conjugate part in a temporary buffer, thereby reducing the FFT memory footprint from 115 KB to 50 KB.

In addition to the accelerometer, a thermistor is used to monitor the temperature every hour. An indication of the state of charge (SoC) is obtained through a measurement reflecting the voltage across the storage element.

B. Communication

The choice of the appropriate communication protocol results from a trade-off between low power consumption, long range, and adequate data rate. Generally, the large volume of raw data generated by an accelerometer (here 250 Hz for 3-axis

corresponds to 73,728 bytes per recording) restricts the choice to high data rate and short-range solutions such as Zigbee, BLE, or Wi-Fi [25][28]. However, owing to the onboard data processing, the amount of useful information is significantly reduced (37 bytes per message), making Low Power Wide Area Network (LPWAN) solutions appropriate while keeping the power consumption low [34]. These technologies such as LoRa or Sigfox can achieve considerable transmission ranges, typically up to 10 km in open-field conditions [35][36]. In this work, LoRa was selected to transfer the processed data every hour to a proprietary gateway.

In the field tests that we considered, the challenge lies in using a single gateway to collect data transmitted by devices deployed on two bridges separated by about 4 km from each other. For logistical reasons, the selected location of the gateway is within a massive building situated 5 km from the more distant bridge. An additional complication arises from the fact that the devices must be mounted on the stay cable, which consists of a steel core. Consequently, the stay cable is likely to induce significant signal losses and to distort the radiation pattern of the transmission antenna.

Two types of antennas were investigated: (i) a high-performance 868 MHz terminal-mount dipole antenna (TI.84.A113) with an SMA connector, and (ii) a PCB monopole antenna described in [37]. The terminal-mount antenna performs very well in free space, making it an ideal solution in areas where there may be no ground plane. The meander-shaped PCB antenna has a medium size (38 × 25 mm²) and provides a low-cost solution with excellent efficiency. Based on the tests described in the next paragraph, the PCB antenna was selected for the final design.

C. Energy harvesting and Power Management

In general, degradation mechanisms in SHM are often extremely slow with effects that manifest after several years, or even decades. For this reason, the system was designed to be fully autonomous and capable of delivering useful information continuously (24/7) without requiring wiring or battery replacement. Although the target structure is expected to undergo vibrations, those induced by external excitations (e.g. traffic, wind) are typically of low intensity and highly stochastic in nature. The photovoltaic energy harvesting is a viable power source except in regions near or beyond the polar circles. However, it is estimated that less than 1 % of the global population resides beyond these latitudes [38]. In this paper, field tests were conducted on two bridges in Belgium, at a latitude of 50°45′.

The average energy supplied by solar panels can be estimated using online calculators [39] based on geographic coordinates, the solar cell type, its spatial orientation (slope, azimuth), system losses, and the time of year (month). This results in an average daily energy output of approximately 386 J for a day in December, under unfavorable orientation conditions imposed by the test setup. The energy storage element used is a hybrid supercapacitor with an estimated stored energy of 120.9 J, which is lower than the average daily energy output for December for the case study. Therefore, the worst-case scenario will be based on the maximum storable energy. The energy consumption of a LoRa or Sigfox transmission depends on several factors, including TX power and the frame duration. At a pre-design stage, it can be assumed that sending one LPWAN message requires approximately 1 J [34]. Considering a target of one message per hour, 24 J (or 7 mWh) are required for the communication which corresponds to approximately one fifth of the stored energy. Whereas the standby current must also be accounted for in the total energy budget, the analysis confirms that the device should sustain continuous operation (24/7, year-round) under the defined configuration parameters. This preliminary calculation will be refined in the following section using data measured under laboratory and field conditions.

We opted for a Power Management Unit (PMU) composed of two stages (see Fig. 1). The first stage consists of a boost converter placed between the solar cell and the supercapacitor. It is protected against overvoltage by a Zener diode and protects the supercapacitor by stopping the charging current once the maximum voltage is reached. The second stage is a buck/boost converter positioned between the supercapacitor and the electronic circuit, in order to provide a sufficient power under a voltage of 3.3 V. This second stage is disabled once the hybrid supercapacitor voltage drops to its minimum value.

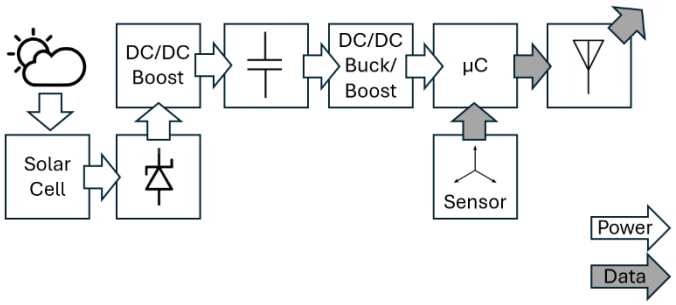

Fig. 1. Block diagram depicting the sensor node with associated power flows and data flows.

D. Integration and packaging

To access to the raw data stored on the microSD card, we selected an off-the-shelf box (rated IP 65) designed for outdoor operation. We selected two materials, acrylonitrile butadiene styrene (ABS) and polycarbonate (PC), in order to compare their machinability on one hand and their performance under operating conditions on the other hand. Basically, the PCB integrates the meandered antenna, the microcontroller, the PMU, the 3-axis accelerometer, and the microSD card.

The solar cell is integrated on the box cover and connected to the PCB through wires. To do so, an aperture was machined in the box cover with a high-precision 3-axis milling machine (DATRON Neo Series 2). A polyurethane resin is then used to ensure a proper sealing (see Fig. 2, left).

To enable optimal mounting of the device onto the cable, a polymer interface part was machined, featuring a V-shaped notch that accommodates different cable diameters. This interface part also allows spacing the antenna from the metal stay cable in order to improve the RF performance of the device. The box is then rigidly fixed to the stay cable using hard-wearing polyamide zip ties passing through the oblong holes of the enclosures (see Fig. 2, right).

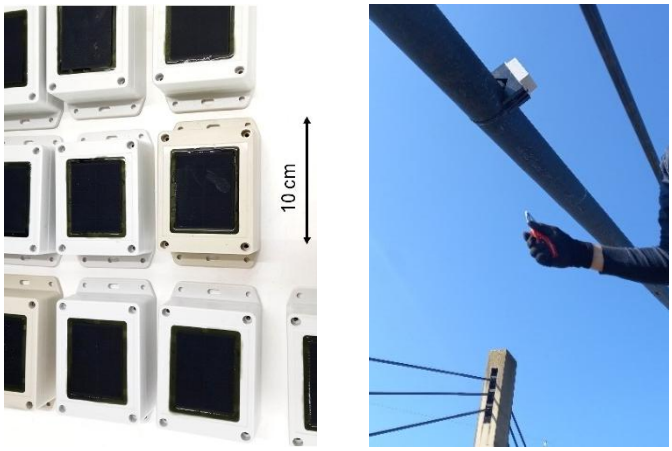

Fig. 2. Left : Assembly and integration of the devices into ABS and PC enclosures. Right: Installation of the sensor on the stay cable.

III. Results

The technology was first validated in the laboratory, and then in the field under real conditions for a period of 5 weeks.

A. Technology validated in lab

1) *Instrumentation*

A validation test was conducted on the integrated system, in which the device was mounted on a TIRAvib vibration generator driven by a BK Precision 4014B function generator. An interface part was manufactured to ensure a robust attachment of the housing to the vibrating platform using six screws. A piezoelectric accelerometer, fixed on the top of the housing, is used as a reference sensor (see Fig. 3). The frequency range studied spans from 1.98 to 60.25 Hz. The measurement results are shown in Fig. 4. The maximum relative error obtained over the entire range is 1.01%. At a frequency of 9.94 Hz, accelerations of 35, 10, and 4 mg were successively applied, first with a sinusoidal signal and then with a square signal, leading to a stable value f_0 of 10.00 Hz delivered by the sensor node. To conclude the test, a sinusoidal excitation at the lowest frequency (1.98 Hz) was applied while gradually reducing the acceleration amplitude. The piezoelectric sensor failed to provide a frequency value below 3 mg, while the sensor node continued to operate correctly down to a lower threshold that could therefore not be determined.

Fig. 3. Laboratory validation of the instrumentation using a vibration shaker.

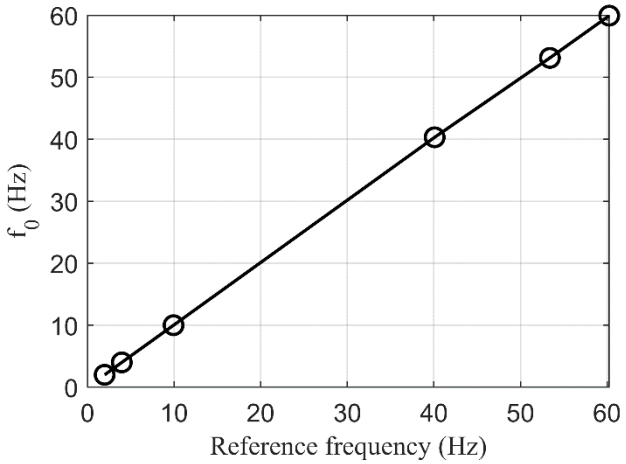

Fig. 4. Fundamental frequency f_0 processed by the embedded firmware as a function of the reference frequency measured by the piezoelectric accelerometer.

2) *Communication*

In the first step, the antenna characterization and optimization were carried out to assess the effect of the stay cable on antenna performance. To this end, 1-meter long cylinders with representative diameters (ranging from 80 – 120 mm) were uniformly covered with aluminum foil to emulate the conductive structure (see Fig. 5). The tuning of the meander-shaped PCB antenna was performed on a bare PCB to avoid damaging an assembled electronic board. After adjusting the length of the PCB antenna, the capacitance and inductance values of the impedance matching circuit were refined through iterative measurements.

Subsequently, free-field measurements revealed that the solar cell negatively affected the antenna's performance. This issue was mitigated by adding a NiZn ferrite tube around the connection leads of the solar cell in order to increase the loop impedance at high frequencies. Indeed, a comparative test was conducted with a 5.1 m distance between the gateway equipped with a vertically oriented dipole antenna and the sensor node, in normal emission mode, placed vertically. The RSSI (signal) values reported by the gateway show a significant improvement, increasing from -59.1 ± 1.1 dBm to -50.8 ± 0.4 dBm when passing the connection leads of the solar cell through a ferrite tube. This results in a significant gain of 8.3 dBm, corresponding to a received power approximately 6.8 times higher, which theoretically translates into an increased communication range by a factor of about 2.6.

Next, radiation patterns were measured for both antenna types by rotating the sensor node through 360° on a turntable, under different configurations, to evaluate the radiation isotropy (see Fig. 6, left). The material used to perform this characterization is a real-time RF spectrum analyzer (Signal Hound BB60C), a broadband antenna (Aaronia HyperLOG 4040), and a Vector Network Analyzer (MEgiq VNA). As an example, the right-hand side of Fig. 6 shows the radiation pattern obtained for the meander-shaped PCB antenna, in continuous-wave mode at 15 dBm, when the device is placed vertically and performs a full rotation around a vertical axis. The distance between the transmitter (sensor node) and the receiver (Aaronia HyperLOG 4040) is set to 5.1 m. The

radiation pattern observed in both horizontal (red curve) and vertical (blue curve) polarizations is relatively isotropic. Based on the satisfactory measurement results, the meander-shaped PCB antenna was selected for the final design because it is low-cost and, above all, its integration is simple and robust, unlike a terminal-mount dipole antenna that requires drilling through the enclosure.

Finally, the impact of the stay cable on the RF transmission performance of the sensor node was characterized as a function of the deployment configuration. In normal emission mode, the received power measured by the RF spectrum analyzer is −32 dBm at 5.1 m without obstacles, −35 dBm when a simulated stay cable is placed 2 cm from the device on the side opposite to the receiver, and −42 dBm when it is positioned between the device and the receiver.

In conclusion, a minimum distance of 2 cm between the stay cable and the PCB antenna is recommended. Depending on the configuration, the attenuation varies significantly, and the best performance is obtained when a line of sight is maintained.

Fig. 5. Study of the stay cable's impact on antenna tunning. The meander-shaped PCB antenna is visible on the right side of the PCB.

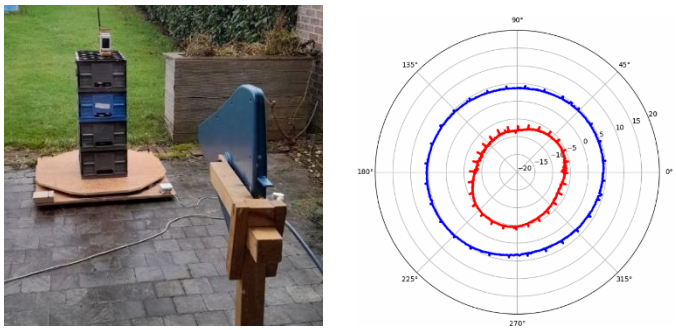

Fig. 6. Left: Characterization of the radiation pattern of the antenna with the device placed vertically on a rotating platform. Right: Radiation pattern of the meander-shaped PCB antenna measured in continuous-wave mode (15 dBm) for a vertically oriented device rotating around a vertical axis. The red and blue curves correspond to horizontal and vertical polarizations, respectively.

3) *Energy Harvesting and Power Management*

First, the current profile has been measured with a Keysight CX3322A current waveform analyzer which reveals a current of 42.4 mA during the data communication over 1.97 s. When supplied with 3.3 V, the corresponding energy is 0.276 J per RF transmission.

Then, we have configured the device to measure, record, process and transmit data every minute to verify how much operations could be performed with a full charge. The device was able to perform 320 operations using stored energy amounting to 120.9 J calculated from the voltage limit values. Neglecting the standby current, this yields 0.378 J per operation: the latter consists in (i) the measurement of the 3-axis accelerations sampled over 32.8 s while saving in the microSD card, (ii) processing the 8192-points FFT for the 3 axis, (iii) searching for the 3 sets of five frequency peaks with the highest magnitudes, and (iv) the LoRa transmission of 37 bytes spread over 2 s. Accordingly, the RF transmission represents about 75 % of the energy needed for an operation.

Finally, the standby current was measured at 89 µA using a Keithley 2000 Multimeter. This corresponds to 25.4 J per day which, added to the energy required to process and transmit data, results in a total energy consumption representing less than one-third of the stored energy. This leaves a comfortable margin either to increase the sampling rate or to operate the device at higher latitudes or on structures that are partly shaded.

B. Tests in operational environment

1) *Communication*

One of the main challenges is to ensure sufficient communication range for connected devices mounted near large metallic structures (stay cables) and near large concrete masses. Three connected accelerometers were installed on the stay cables of the Lixhe Bridge and three additional units on the Lanaye Bridge (Belgium). The gateway, equipped with a dipole antenna and held by an operator under outdoor conditions, demonstrated reliable data receiving at distances up to 7.2 km. This range would theoretically cover an area encompassing several bridges with a single gateway. Furthermore, there remains significant potential for improvement since the gateway can be elevated above ground level and equipped with a higher-gain antenna. However, for logistical reasons and easier data access, the gateway (depicted by a green square in Fig. 7) was installed inside a concrete building, meaning that the signal attenuation is significant. Nevertheless, the signals transmitted by the devices installed on the Lanaye Bridge (1.2 km from the gateway) and the Lixhe Bridge (5.1 km from the gateway) show received signal strength indication (RSSI) values of approximately –95 dB and –135 dB, respectively. The last value is close to the reception threshold but remains sufficient for reliable data reception. This is in good agreement with the gateway's sensitivity (−137 dBm for a Spreading Factor SF = 12).

Fig. 7. The sensors fixed on the Lanaye Bridge and the Lixhe Bridge are respectively represented by red triangles and yellow circles. The gateway is placed inside a building and is represented by a green square.

2) *Energy Harvesting and Power Management*

The placement of the enclosures were adjusted to optimize the antenna orientation. Since the antenna is fixed to the enclosure, the degrees of freedom are limited. The enclosure can only be rotated around the cable axis, as long as the solar cell is not facing the ground. As a result, the photovoltaic cells were positioned at a highly unfavorable orientation, facing north-northeast with a slope angle of approximately 60° (NB: optimal slope = 35°).

The device measures and transmits the voltage level of the hybrid supercapacitor to provide information on the state of charge. The energy storage element operates within a voltage range of 2.6 V to 3.85 V. The voltage recorded over roughly a 5 week-period (20 March 2025 – 23 April 2025) show minimum values of 3.75 V for most devices. As an approximation, the voltage profile is periodic and exhibits a trapezoidal shape composed of three phases: fast charging, clamping, and discharging. The discharge phase is nearly linear and lasts approximately 12 hours. The resulting discharge depth is only 8 %, corresponding to a supplied energy of 11.4 J. From laboratory characterizations, the energy required for 12 operations is 4.5 J, while 12.7 J are consumed over 12 hours by the standby current, making a total of 17.2 J of energy consumed. Expressed in terms of average power, we obtain 104 µW, 294 µW and 398 µW for the data operation, the standby current and the total respectively. The values for the extracted energy were in good agreement with the consumed energy.

In practice, the solar cell may accidentally be covered for a short period (e.g. snow, dead leaf). It is therefore relevant to estimate the maximum achievable autonomy of the system in the absence of illumination. From the average overall power estimation (398 µW), the backup mode autonomy is estimated at 3.5 days to use up the total amount of stored energy (i.e. 120.9 J for a full charge).

3) *Instrumentation*

The validity and reliability of the data are essential for assessing the structural health of the bridge, in particular for enabling continuous monitoring of the tension in the stay cables. In practice, due to logistical constraints, the accelerometers had to be installed relatively close to the lower anchorage point of the stay cables which corresponds to an unfavorable location (low vibration, higher-order harmonics). The embedded firmware developed on the microcontroller performs a FFT on data sampled at 250 Hz over a window of 32.8 seconds for the three axes. Peak identification is then carried out, followed by ranking in decreasing order of magnitude. Only the five most prominent peaks for each axis are transmitted. The value sent for the 5 main frequencies vary from one sample to another since the frequency content is particularly rich due to the sensor location (near the anchorage point). Hence, for each sensor, we obtain more than a dozen harmonics after several transmissions.

If the sensor was placed at mid-span, the vibration signal would have been easier to measure (maximum displacements) on one hand, and the frequency content would be composed primarily of the fundamental frequency and odd harmonics (vibration antinodes) on the other hand.

The stay cables are naturally excited by external stimuli, namely traffic or wind. Thanks to the high sensitivity of the accelerometer, even very low-amplitude vibrations (typ. 1 mg) can be detected, allowing the embedded algorithm to extract the five dominant frequencies. However, in certain cases, vibrations are almost nonexistent in the absence of external excitation. Under purely static conditions, the algorithm then returns five zero frequencies. Over the duration of the test, conducted over five weeks with six devices evenly distributed across the two bridges, between 71 % and 84 % of the samples yielded meaningful frequency content, demonstrating the high sensitivity rate for the devices.

Fig. 8 displays the packets of the five dominant frequencies transmitted hourly over approximately five weeks. The most significant frequency in each packet is represented by an open blue circle (labeled ‘#1’). A series of regularly spaced lines can be observed, corresponding to the main harmonics which are multiples of the fundamental frequency. This fundamental frequency, measured for the device labeled *Lanaye_M* (mid-span cable of the Lanaye Bridge), is 1.35 Hz. For this particular sensor node, the fundamental frequency rarely appears. Data points at 0 Hz reflect unexploitable vibrations, corresponding to quasi-static conditions. The proportion of these specific points relative to the total number of points affects the sensitivity rate.

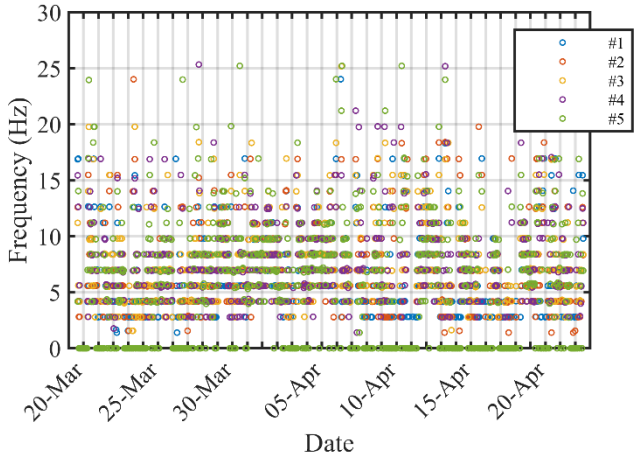

Fig. 8. Distribution of the five dominant frequencies obtained for the device Lanaye_M. The data are ranked in decreasing order of importance, with #1 corresponding to the highest measured amplitude and #5 to the lowest.

These data are presented differently in the histogram shown in Fig. 9, where each received frequency is binned into intervals width of 0.05 Hz. The frequency peaks are displayed according to their normalized occurrence, as zero values (non-measurable data) have been excluded. As expected, the peaks correspond to integer multiples of the fundamental frequency. The most frequently observed peak, also associated with the highest amplitude, occurs at 6.95 Hz (5th harmonic). Whereas the peaks are relatively well defined, the frequencies may vary depending on the loading conditions at the time of measurement. For instance, the passage of heavy vehicles or a drop in ambient temperature can lead to an increase in cable tension, resulting in a higher fundamental frequency. Fig. 9 is limited to the representation of the first 12 prominent peaks, although additional peaks could have been displayed.

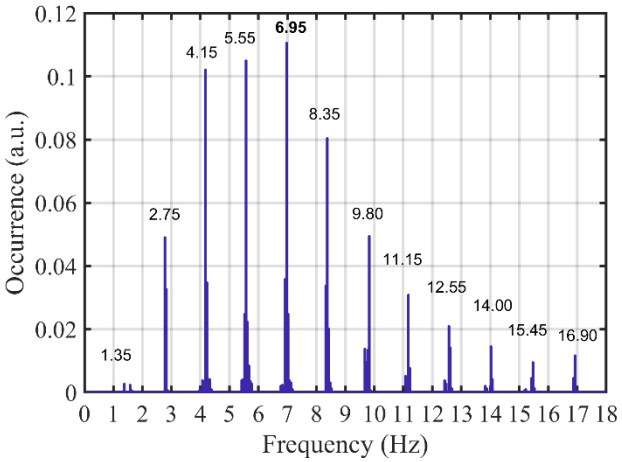

Fig. 9. Frequency spectrum obtained for the device Lanaye_M.

For the mid-span cable monitored on the Lixhe Bridge (see Fig. 10), the frequency spectrum exhibits a noticeably different pattern, with low frequencies being predominant. The spread of the peaks is more pronounced than in Fig. 9. The harmonics still correspond to multiples of the fundamental frequency which is 2.50 Hz.

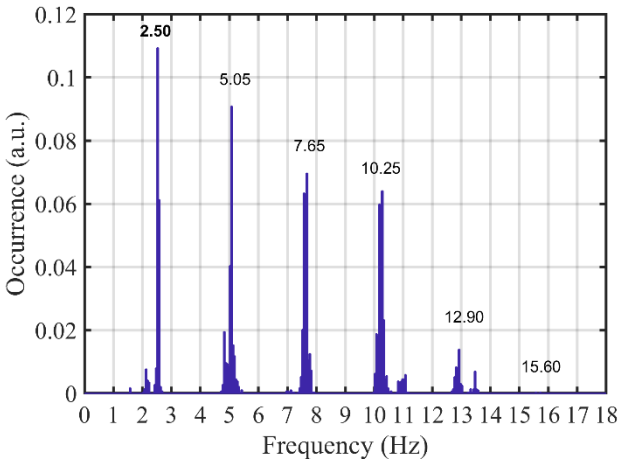

Fig. 10. Frequency spectrum obtained for the device Lixhe_M.

At the end of the measurement campaign, we extracted the microSD card from one of the devices. From the raw data stored on the microSD card, we performed a FFT using the Matlab® software. It results that the peak values obtained by the firmware are consistent with those provided by Matlab. However, the frequency content generated by Matlab is richer and reveals a larger number of peaks (floating-point accuracy).

Fig. 11 shows the evolution of the frequencies corresponding to the second and third harmonics for device labeled *Lanaye_S* (short stay cable, Lanaye Bridge) as a function of the temperature. Over the test campaign, the recorded temperatures range from −5.5 °C to 22.5 °C. As expected, it can be observed that the tension – reflected by the frequency – increases as the temperature decreases [21].

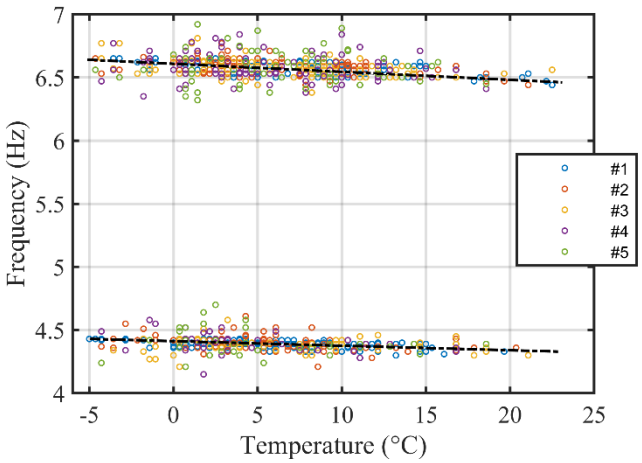

Fig. 11. Evolution of the 2nd and 3rd harmonics as a function of temperature for the device Lanaye_S.

IV. Discussion

During the test period, several episodes of freezing temperatures and intense rainfall occurred. By the end of the test campaign, all sensor units remained fully operational. Indeed, after opening the enclosures, no signs of moisture ingress were observed.

Table 1 summarizes the key results obtained during the test period. The six sensors, labelled with the site name and a size code (S, M, or L) based on the cable length, are distributed 3 per bridge. Then, characteristics of the stay cable (L and μ in relation with (1)) are given. Basically, the stay cables of Lanaye appear to be more slender and exhibit different cross-sections.

The fundamental frequency obtained by our sensor nodes is denoted f_0 whereas f_0' refers to the reference value. The reference values (f_0') come from measurements conducted several months prior to our test campaign using commercially available and battery powered sensor nodes connected via WiFi and a FFT performed remotely (with high computational power and floating-point accuracy). Except for *Lanaye_L*, the small relative difference between f_0 and f_0' is about ± 2 %, that provides full validation of the instrumentation and processing chain. As for the device *Lanaye_L*, this relative difference reaches – 6.5 %.

The dominant frequency corresponds to the highest vibration amplitude observed over the entire duration of the test campaign. For the Lixhe Bridge, the dominant frequency always correspond to the fundamental frequency. In opposition, for the Lanaye Bridge (slender stay cables), the dominant frequency correspond to the 3rd or 5th harmonic. As a reminder, the frequency content depends on the accelerometer's relative position along the total length of the stay cable.

According to (1), we calculated the current tension T from the value f_0. Compared with the Lanaye Bridge, the tension of the stay cables in Lixhe are significantly higher and have values around 3.5×10^6 N. Knowing f_0 and f_0', the tension loss for the longest stay cable (*Lanaye_L)* is estimated at 12 %. Consequently, this stay cable requires special attention.

We have defined the sensitivity rate (SR) as a parameter indicating the percentage of samples that yield non-zero values for the dominant frequencies. Without sustained excitation (e.g. shaker, unbalance moment...), the vibrations expected in the stay cables are inherently fluctuating and of low amplitude, or even absent. In practice, the presence of vibrations during the 32.8-second sampling window depends on the occurrence of external stimuli (traffic, wind, rain-wind) at that time. If the vibration signal is too low or nonexistent, the information transmitted by the node is then limited to temperature and state of charge. This is not critical, but a high SR is desirable to enable regular tension monitoring. Overall, the SR is of 80 % meaning that 8 samples over 10 returns the 5 main frequencies of the vibration. It is also worth noting that the shortest stay cables (*Lanaye_S* and *Lixhe_S*) exhibit a lower SR as they are more difficult to excite. Considering that sampling occurs every hour and that almost 8 out of 10 samples are exploitable, the target of at least 4 measurements per day is met, and even largely exceeded.

The minimum state of charge (SoC) is given in the table. It is obtained from the lowest voltage measured across the storage element during the test campaign. For all 6 devices, the values are consistent, with around 8 % depth of discharge. For several reasons (antenna orientation, cable slope), the orientation of the solar cells naturally differ from one installation to another. However, the enclosure positioning does not appear to be critical in terms of energy harvesting even if positioned under unfavorable conditions (near-vertical, facing north-northeast). This is an excellent result as it significantly simplifies the installation process.

When the RSSI measured at the gateway is higher than −135 dBm, no packet loss was observed out of around 800 transmissions per device. For the Lixhe Bridge, located 5 km from the gateway, two devices report RSSI values close to the gateway's sensitivity threshold (−137 dBm for SF = 12), with a packet loss rate of approximately 40 to 70 %. Nevertheless, the generated information, though limited, remains fully usable.

TABLE I
SUMMARY TABLE OF KEY VALUES RECORDED ON THE 6 DEVICES DURING THE TEST CAMPAIGN

Device	L (m)	μ (kg/m)	f_0 (Hz)	f_0' (Hz)	T (kN)	SR (%)	SoC (%)	RSSI (dB)
Lanaye_S	49.3	43.8	2.25	2.20	2156	71	92	-95
Lanaye_M	82.5	43.8	1.35	1.39	2173	84	92	-94
Lanaye_L	122	78.2	0.75	0.80	2619	83	92	-92
Lixhe_S	34.9	75.2	3.10	3.05	3520	75	89	-136
Lixhe_M	42.6	75.2	2.50	2.55	3412	82	92	-131
Lixhe_L	50.6	75.2	2.20	2.16	3728	84	91	-137

V. CONCLUSION

We have developed a plug-and-forget sensor node dedicated to structural health monitoring, addressing key technological barriers such as measurement accuracy, device power supply, and data transmission. The device is built around a high-precision 3-axis accelerometer with onboard data processing. Processed data is transmitted via LoRa over 5 km in semi-obstructed environments (7.2 km in open space) despite large metallic cables close to the antenna. Following successful laboratory validation, field tests were conducted on cable-stayed bridges with the objective of monitoring cable stay tension via vibration analysis. The results, benchmarked with a reference instrumentation system, validate the measurement method, despite an unfavorable sensor placement (near the anchorage point). The high sensitivity of the sensor node enables reliable detection of the frequency content of the vibration – provided that an external stimulus (e.g., traffic, wind, combined rain-wind) occurs during sampling – and yields an average sensitivity rate of 8 samples out of 10. Despite unfavorable orientation of the solar cells (near-vertical, north-northeast), the system is fully autonomous and can operate 24/7 thanks to a compact solar cell (28 cm²) and the optimization of both hardware and firmware. The analysis shows that a significant operational margin remains, which could either be used to increase the sampling rate or to consider deploying the sensor node in regions with very low solar irradiance. All sensors remained operational despite freezing temperatures and heavy rainfall, with no moisture ingress observed. Finally, the deployed instrumentation allowed the early detection of tension loss in one of the monitored cables. This instrumentation system is remarkably easy to use: it is quick to install, requires zero maintenance, and directly provides useful information (processed data). Demonstrated here on cable-stayed bridges, the technology could easily be applied for other structural health monitoring use cases or in the industrial sector.

ACKNOWLEDGMENT

The authors would like to thank V2i SA (Liège, Belgium) for their assistance in the instrumentation characterization, eFFiciency research SRL (Liège, Belgium) for their support in the antenna characterization, and SPW/Department of Structural Expertise (Liège, Belgium) for granting site access and facilitating the deployment of the solution.

REFERENCES

1. Wu, Z., Nagayama, T., Dang, J., & Astroza, R. Experimental Vibration Analysis for Civil Engineering Structures. 2021
2. Abdulkarem, M., Samsudin, K., Rokhani, F. Z., & A Rasid, M. F. (2020). Wireless sensor network for structural health monitoring: A contemporary review of technologies, challenges, and future direction. *Structural health monitoring*, *19*(3), 693-735.
3. Saidin, S. S., Jamadin, A., Abdul Kudus, S., Mohd Amin, N., & Anuar, M. A. (2022). An overview: The application of vibration-based techniques in bridge
4. Plevris, V., & Papazafeiropoulos, G. (2024). AI in Structural Health Monitoring for Infrastructure Maintenance and Safety. *Infrastructures*, *9*(12), 225.
5. Biondi, F., Addabbo, P., Clemente, C., & Orlando, D. (2021, March). A new paradigm to observe early warning faults of critical infrastructures by micro-motion estimation from satellite SAR observations. Application to pre-collapse damage assessment of the Morandi bridge in Genoa (Italy). In *EUSAR 2021; 13th European Conference on Synthetic Aperture Radar* (pp. 1-5). VDE.
6. Long, A. E., Basheer, P. A. M., Taylor, S. E., Rankin, B. G., & Kirkpatrick, J. (2008, December). Sustainable bridge construction through innovative advances. In *Proceedings of the Institution of Civil Engineers-Bridge Engineering* (Vol. 161, No. 4, pp. 183-188). Thomas Telford Ltd.
7. Kamariotis, A., Chatzi, E., & Straub, D. (2023). A framework for quantifying the value of vibration-based structural health monitoring. *Mechanical Systems and Signal Processing*, *184*, 109708.
8. He, Z., Li, W., Salehi, H., Zhang, H., Zhou, H., & Jiao, P. (2022). Integrated structural health monitoring in bridge engineering. *Automation in construction*, *136*, 104168.
9. Wu, W. H., Chen, C. C., Lin, S. L., & Lai, G. (2023). A Real-Time Monitoring System for Cable Tension with Vibration Signals Based on an Automated Algorithm to Sieve Out Reliable Modal Frequencies. Structural Control and Health Monitoring, 2023(1), 9343343.
10. Tsuchimoto, K., Narazaki, Y., Hoskere, V., & Spencer, B. F. (2021). Rapid postearthquake safety evaluation of buildings using sparse acceleration measurements. Structural Health Monitoring, 20(4), 1822-1840.
11. Zarbaf, S. E. H. A. M., Norouzi, M., Allemang, R., Hunt, V., Helmicki, A., & Venkatesh, C. (2018). Vibration-based cable condition assessment: A novel application of neural networks. Engineering Structures, 177, 291-305.conditions in cables. Journal of Sound and Vibration, 511, 116326.
12. "Uplift of the Lixhe bridge", Bureau Greisch, Seraing, Liege, Belgium, 2018, Available: https://www.greisch.com/en/uplift-of-the-lixhe-bridge-bureau-greisch-busy-to-analyse-the-stability-of-the-structure/
13. Geuzaine, M., Foti, F., & Denoël, V. (2021). Minimal requirements for the vibration-based identification of the axial force, the bending stiffness and the flexural boundary
14. Kim, B. H., & Park, T. (2007). Estimation of cable tension force using the frequency-based system identification method. Journal of sound and Vibration, 304(3-5), 660-676.
15. Weng, J., Chen, L., Sun, L., Zou, Y., Liu, Z., & Guo, H. (2023). Fully automated and non-contact force identification of bridge cables using microwave remote sensing. Measurement, 209, 112508.
16. Ni, Y. Q., Wang, X. Y., Chen, Z. Q., & Ko, J. M. (2007). Field observations of rain-wind-induced cable vibration in cable-stayed Dongting Lake Bridge. Journal of Wind Engineering and Industrial Aerodynamics, 95(5), 303-328.
17. Sun, L., Chen, L., & Huang, H. (2022). Stay cable vibration mitigation: A review. Advances in Structural Engineering, 25(16), 3368-3404.
18. Jiang, C., Wu, C., Cai, C. S., & Xiong, W. (2020). Fatigue analysis of stay cables on the long-span bridges under combined action of traffic and wind. Engineering Structures, 207, 110212.
19. Guo, J., & Zhu, X. (2020). Field monitoring and analysis of the vibration of stay cables under typhoon conditions. Sensors, 20(16), 4520.
20. Bono, F. M., Polinelli, A., Radicioni, L., Benedetti, L., Castelli-Dezza, F., Cinquemani, S., & Belloli, M. (2025). Wireless Accelerometer Architecture for Bridge SHM: From Sensor Design to System Deployment. Future Internet, 17(1), 29.
21. Nguyen, K. D., Kim, J. T., & Park, Y. H. (2013). Long-term vibration monitoring of cable-stayed bridge using wireless sensor network. International Journal of Distributed Sensor Networks, 9(11), 804516.
22. Jana, D., Nagarajaiah, S., Yang, Y., & Li, S. (2022). Real-time cable tension estimation from acceleration measurements using wireless sensors with packet data losses: Analytics with compressive sensing and sparse component analysis. Journal of Civil Structural Health Monitoring, 1-19.
23. Giammarini, M., Isidori, D., Concettoni, E., Cristalli, C., Fioravanti, M., & Pieralisi, M. (2015, April). Design of wireless sensor network for real-time structural health monitoring. In 2015 IEEE 18th International Symposium on Design and Diagnostics of Electronic Circuits & Systems (pp. 107-110). IEEE.
24. Kurata, M., Kim, J., Lynch, J. P., Van Der Linden, G. W., Sedarat, H., Thometz, E., ... & Sheng, L. H. (2013). Internet-enabled wireless structural monitoring systems: development and permanent deployment at the New Carquinez Suspension Bridge. *Journal of structural engineering*, *139*(10), 1688-1702.
25. Jeong, S., Lee, Y. J., Shin, D. H., & Sim, S. H. (2019). Automated real-time assessment of stay-cable serviceability using smart sensors. Applied Sciences, 9(20), 4469.
26. Zanelli, F., Castelli-Dezza, F., Tarsitano, D., Mauri, M., Bacci, M. L., & Diana, G. (2021). Design and field validation of a low power wireless sensor node for structural health monitoring. Sensors, 21(4), 1050.
27. López-Castro, B., Haro-Baez, A. G., Arcos-Aviles, D., Barreno-Riera, M., & Landázuri-Avilés, B. (2022). A systematic review of structural health monitoring systems to strengthen post-earthquake assessment procedures. Sensors, 22(23), 9206.
28. Sivagami, A., Jayakumar, S., & Kandavalli, M. A. (2020, October). Structural health monitoring using smart sensors. In AIP Conference Proceedings (Vol. 2281, No. 1). AIP Publishing.
29. Sonbul, O. S., & Rashid, M. (2023). Towards the structural health monitoring of bridges using wireless sensor networks: A systematic study. Sensors, 23(20), 8468.
30. Sazonov, E., Li, H., Curry, D., & Pillay, P. (2009). Self-powered sensors for monitoring of highway bridges. IEEE Sensors Journal, 9(11), 1422-1429.
31. Palagummi, S. V., & Yuan, F. G. (2017). An enhanced performance of a horizontal diamagnetic levitation mechanism–based vibration energy harvester for low frequency applications. Journal of Intelligent Material Systems and Structures, 28(5), 578-594.
32. Liu, Y., Voigt, T., Wirström, N., & Höglund, J. (2018). Ecovibe: On-demand sensing for railway bridge structural health monitoring. IEEE Internet of Things Journal, 6(1), 1068-1078.
33. Chen, Y., Qin, L., Zou, Y., Sun, L., Chen, L., & Chen, S. (2025). Simplification and improvement of cable tension identification based on effective vibration length estimated from multiple sensors located near one support. Measurement, 242(A), 115755.
34. Joris, L., Dupont, F., Laurent, P., Bellier, P., Stoukatch, S., & Redouté, J. M. (2019). An autonomous sigfox wireless sensor node for environmental monitoring. IEEE Sensors Letters, 3(7), 01-04.
35. Augustin, A., Yi, J., Clausen, T., & Townsley, W. M. (2016). A study of LoRa: Long range & low power networks for the internet of things. Sensors, 16(9), 1466.
36. Petajajarvi, J., Mikhaylov, K., Roivainen, A., Hanninen, T., & Pettissalo, M. (2015, December). On the coverage of LPWANs: range evaluation and channel attenuation model for LoRa

technology. In 2015 14th international conference on its telecommunications (itst) (pp. 55-59). IEEE.
37. Texas Instruments, "Monopole PCB Antenna with Single or Dual Band Option" Application Report SWRA227E, 2017. [Online]. Available: https://www.ti.com/lit/an/swra227e/swra227e.pdf
38. Kummu, M., & Varis, O. (2011). The world by latitudes: A global analysis of human population, development level and environment across the north–south axis over the past half century. Applied geography, 31(2), 495-507.
39. European Commission, "PHOTOVOLTAIC GEOGRAPHICAL INFORMATION SYSTEM", [Online].Available:https://re.jrc.ec.europa.eu/pvg_tools/en/

Philippe Laurent received the M.Sc. degree in electromechanical engineering from the University of Liège, Belgium, in 2002, and the Ph.D. degree in measurement and instrumentation from the same university in 2009, with research focused on thermal effects in superconductors.
He then worked as a Materials and Process Engineer in the aeronautics sector at Safran Aero Booster, Liège. In 2010, he joined the Microsys Laboratory, University of Liège, as a Research Engineer. In March 2016, he was part of the team that won the Little Box Challenge, an international power electronics competition organized by Google and the IEEE Power Electronics Society. His current research interests include ultra-low-power IoT systems.
Mr. Laurent received the first prize at the 5G World 2016 Innovation Accelerator, London, in June 2016.

Pierre Bellier received the M.Sc. degree in electrical and electronics engineering and the M.Sc. degree in computer engineering from the University of Liege, Liege, Belgium, in 2006 and 2008, respectively. In October 2008, he joined the Microsys Laboratory, University of Liege, as a Research Engineer. He worked on various projects, including research, industrial, smart buildings, medical, and the Internet-of-Things (IoT) applications. His research interests include connected sensor systems, energy-efficient electronic design, embedded software programming, and power-optimized wireless communication.

François Dupont received the M.Sc. degree in electrical and electronics engineering from the University of Liège, Liège, Belgium, in 2007.
He subsequently joined the Microsys Laboratory, University of Liège, as a Research Engineer in 2008. Since then, he has participated in about ten projects whose objectives were the integration/miniaturization of sensor systems. He is currently a Team Leader of the Microsys Laboratory, whose research topics are energy harvesting, connected sensors system, and advanced packaging. His core competence is the design of miniaturized and ultralow-power electronic circuits.

Jean-Michel Redouté (M'09-SM'12) received the M.S. degree in electronics from the University College in Antwerp, Antwerp, Belgium, in 1998, and the M.Eng. degree in electrical engineering from the University of Brussels, Brussels, Belgium, in 2001.
In August 2001, he started working at Alcatel Bell, Antwerp, where he was involved in the design of analog microelectronic circuits for telecommunications systems. In January 2005, he joined the University of Leuven, Leuven, Belgium, as a Ph.D. Research Assistant. In May 2009, he presented his Ph.D. entitled "Design of EMI resisting analog integrated circuits." In September 2009, he started working at the Berkeley Wireless Research Center at the University of California at Berkeley, Berkeley, CA, USA: this research was funded by the Belgian American Educational Foundation (BAEF). In September 2010, he joined Monash University, Melbourne, VIC, Australia, as a Senior Lecturer. In July 2018, he started working at the University of Liège, Liège, Belgium, as an Associate Professor. His research is concentrated on miniaturized and low-power sensor interfaces, robust mixed-signal integrated circuit (IC) design with a high immunity to electromagnetic interference (EMI), biomedical (integrated and nonintegrated) circuit design, energy harvesting, and integrated imagers.
Mr. Redouté is an Associate Editor of the IEEE SENSORS JOURNAL.